




Insights into the effects of modifying factors on the solvent-free synthesis of FeAPO-5 catalysts towards phenol hydroxylation

Xinhong Zhao¹  · Weiting Duan¹ · Xiaoxiao Zhang¹ · Dong Ji¹ · Yu Zhao¹ · Guixian Li¹

Received: 29 May 2018 / Accepted: 5 September 2018 / Published online: 8 September 2018
© Akadémiai Kiadó, Budapest, Hungary 2018

Abstract

A modified solvent-free method has been developed to synthesize FeAPO-5 zeolite catalysts with hierarchical porous structure as well as high crystallinity and iron content. The effects of mechanochemical and low-temperature pretreatment, as well as the addition of hydrogen peroxide and seed crystals on the synthesis of FeAPO-5 were studied in detail. The composition and structural features of relatively pure resultant products were deeply analyzed by XRD, SEM, ICP-AES, CHN analysis, TG-DTA, UV-Vis diffuse reflectance spectroscopy and N₂ physisorption. Most importantly, low-temperature pretreatment towards H₂O₂-containing precursor mixtures can to a great degree improve the crystallinity of FeAPO-5 molecular sieve. Significantly, compared to the conventional micron-sized microporous FeAPO-5 zeolite, the hierarchical FeAPO-5 catalysts created by this modified solvent-free method show superior performance in phenol hydroxylation, in which the one with a high content of framework iron species exhibits the best catalytic performance, giving phenol conversion of about 40% and dihydroxybenzene selectivity of up to 80% at 50 °C within 3 h reaction time.

Keywords Mechanochemical pretreatment · Low-temperature pretreatment · Hydrogen peroxide · Seed crystals · Solvent-free synthesis · Phenol hydroxylation

Electronic supplementary material The online version of this article (<https://doi.org/10.1007/s11144-018-1465-2>) contains supplementary material, which is available to authorized users.

✉ Xinhong Zhao
licpzhaoxh@lut.cn

¹ School of Petrochemical Engineering, Lanzhou University of Technology, Lanzhou 730050, People's Republic of China

Introduction

Aluminophosphate molecular sieves (AlPO₄-based) as the third generation of molecular sieve family, which were first synthesized in 1982, recently attracted much attention from the researchers [1, 2]. Owing to their unique frameworks with pores and channels, they have been widely used in various areas of chemical industry such as adsorption and separation, ion exchange and catalysis [3–8]. Generally, these fascinating materials can be synthesized by several synthesis methods, including hydrothermal/solvothermal and ionothermal synthesis [9–11]. Notably, these synthesis methods are usually carried out in the presence of solvents, and the use of solvents normally produces large amounts of waste and generates high pressure.

In recent years, Xiao and co-workers reported that some aluminosilicate and aluminophosphate zeolites can be synthesized via a solvent-free route [12–15]. Solvent-free synthesis is a novel method, in which no additional solvent is introduced in the reaction system. This synthetic method exhibits many advantages such as high synthesis yield, low pollution and preparation cost. Particularly, these AlPO₄-based zeolites synthesized by the solvent-free route are hierarchical porous materials, which are very favorable for enhancing their catalytic performance [15]. In our laboratory, AFI-, CHA-, and AEL-type aluminophosphate molecular sieves have been successfully synthesized via this solvent-free route [16–18]. However, few attempts have been made on the solvent-free synthesis of metal-containing zeolites, especially those with hierarchical porous structure and high metal content as well as high crystallinity. It is well known that these structural characteristics and properties are of crucial importance for a high-performance zeolite catalyst.

Recently, several approaches, including mechanochemical and low-temperature pretreatment, as well as the addition of hydrogen peroxide and seed crystals, were adopted to tune the nucleation and growth rate of zeolite crystals, aiming to obtain zeolite materials with peculiar structure or properties [19–22]. Wakihara and co-workers reported that Silicalite-1 zeolites with high manganese content can be successfully prepared from mechanochemically pretreated reactants [19]. Mintova considered that the low-temperature synthesis of zeolites below 120 °C favors nucleation over crystal growth, thus resulting in the formation of nanocrystals [20]. Yu's group found that the nucleation stage of zeolite can be prominently accelerated by hydroxyl free radical in situ generated from Fenton reaction [21]. As for seed crystals, one had ever used them to increase the crystallization rate or control the purity and properties of zeolites [22]. It is worth noting that, to this day, there is no report indicating the effect of these modifying factors on solvent-free system.

Inspired by the above significant findings, herein we present a solvent-free process to synthesize hierarchical FeAPO-5 molecular sieves with high crystallinity and iron content through mechanochemical and low-temperature pretreatment route, as well as assisted by hydrogen peroxide and seed crystals. The absence of water greatly reduces the environmental pollution and improves the yield of hierarchical FeAPO-5. Furthermore, the obtained zeolite with a hierarchical structure including micro-, meso- and macro-pores can enhance the mass transport. As a result, a much

higher catalytic activity than that of the conventional FeAPO-5 catalyst in phenol hydroxylation was observed. This method provides a new insight into hierarchical zeolite synthesis which only involves a simple pretreatment process without solvent, and thus has potential for the preparation of hierarchical zeolite catalysts at the industrial level.

Experimental sections

Materials

In the present synthesis, all reagents were of reagent grade and used without further purification: tetraethylammonium bromide (denoted as TEABr, Aladdin Reagent), dipropylamine (denoted as DPA, Sinopharm Chemical Reagent Co. Ltd, China), pseudo-boehmite (Shandong Zibo Senchi Chemical Co. Ltd, China), phosphoric acid (H_3PO_4 , 85 wt% in water, Yantai Shuangshuang Chemical Reagent Co. Ltd, China), ferric citrate ($\text{FeC}_6\text{H}_5\text{O}_7 \cdot \text{H}_2\text{O}$, Aladdin Reagent), ferric nitrate ($\text{FeNO}_3 \cdot 9\text{H}_2\text{O}$, Tianjin Kaixin Chemical Industry Co. Ltd, China), ammonium ferric citrate (Sinopharm Chemical Reagent Co. Ltd), ferric chloride (FeCl_3 , Xilong Chemical Co. Ltd, China), hydrogen peroxide (H_2O_2 , 30 wt% in water, Sinopharm Chemical Reagent Co. Ltd), acetone (Beijing Chemical Plant, China) and deionized water. Two kinds of seed crystals (denoted as SC), whose sizes are respectively in the range of nanometer and micrometer, were used in the subsequent synthesis.

Synthesis of FeAPO-5

General synthesis procedure of FeAPO-5: TEABr, DPA, pseudo-boehmite (0.838 g), H_3PO_4 , iron sources, H_2O_2 and 0.1 g of seed crystals if required, were measured out in a molar ratio of 1.0 Al_2O_3 :0.762 P_2O_5 :0.1 Fe_2O_3 :1.524 DPA:0.2 TEABr:0.2 H_2O_2 and ground in a mortar for 20 min (the other mixing procedure was as follows: pseudo-boehmite, H_3PO_4 and iron sources were first milled in a ball mill (XQM-0.4L, speed of rotation 400 rpm, Changsha Tencan Powder Technology Co. LTD, China) for 1 h, then the obtained composite were mixed with the remaining starting materials, subjected to hand grinding in a mortar for another 20 min). The resultant precursor mixture was transferred to 50 mL Teflon-lined stainless-steel autoclaves and crystallized under static conditions at 200 °C for 36 h (or first pretreated at low temperature of 80 °C for 24 h before high-temperature crystallization). After the synthesis mixture had cooled to room temperature, large amounts of deionized water were dumped into the Teflon bottle to dissolve the unreacted starting materials. The resulting solid product was recovered by centrifugation, washed with deionized water and acetone, and then dried in air at 110 °C. The template in the as-synthesized samples were removed by calcination at 550 °C for 5 h. Final samples were designated as Fe_x -Hand, Fe_x -Mech, Fe_x -Hand-LT, Fe_x HP-Hand, Fe_x HP-Mech, Fe_x HP-Hand-LT, Fe_xSC_y -Hand, Fe_xSC_y -Mech, Fe_xSC_y -Hand-LT, where Fe represents the iron sources; “LT”, “HP” and “SC” were the abbreviations of low-temperature pretreatment, hydrogen peroxide and

seed crystals, respectively; “x” and “y” represent the types of iron sources and seed crystals; “Hand” and “Mech” indicate that the starting materials were hand-mixed and mechanochemically treated, respectively. For comparison purpose, a FeAPO-5 reference sample (denoted as FeAPO-5-Hydro) was synthesized by conventional hydrothermal method according to the literature [23]. Detailed names and synthesis conditions of the FeAPO-5 samples were presented in Table 1.

Characterization

Powder X-ray diffraction (XRD) patterns of the as-synthesized materials were performed on a D/Max-2400 Rigaku diffractometer with Cu K_{α} radiation operated at 40 kV and 150 mA. The crystallinities of the FeAPO-5 samples were calculated according to the intensity of the peaks at 2θ of 7.5°, 14.9°, 19.8°, 21.1°, 22.5° and 26.0° [24]. Scanning electron microscopic (SEM) images were obtained from JSM-6701F instruments. Nitrogen adsorption/desorption studies were conducted on a Micromeritics ASAP 2010 surface area and pore size analyzer at - 196 °C. Samples were outgassed at 350 °C for 4 h prior to the measurements. Specific surface areas of the specimens were calculated from the adsorption data obtained at p/p_0 between 0.06 and 0.20, using the Brunauer–Emmett–Teller (BET) equation. The micropore volumes were determined by the t-plot method. The content of iron in the final product was quantified by IRIS Advantage Inductively Coupled Plasma Atomic

Table 1 Sample notations, phases, crystallinity and iron content of synthesized products

Sample ^a	Product phases	I_{002}/I_{100}^b	Crystallinity (%)	Iron content (wt%) ^c
Fe ₁ -Hand	AFI CHA + dense phase	–	–	–
Fe ₂ -Hand	AFI \gg CHA + dense phase	–	–	–
Fe ₃ -Hand	AFI \gg CHA + dense phase	–	–	–
Fe ₄ -Hand	AFI	0.966	84.4	6.08
Fe ₄ -Mech	AFI > CHA + cristobalite	–	41.4	–
Fe ₄ -Hand-LT	AFI	0.753	72.8	5.88
Fe ₄ HP-Hand	AFI + CHA + dense phase	–	41.2	–
Fe ₄ HP-Hand-LT	AFI \gg CHA	0.803	100	5.10
Fe ₄ HP-Mech	AFI + CHA + dense phase	–	50.5	–
Fe ₄ SC _n -Hand	AFI \gg CHA	0.688	47.3	5.40
Fe ₄ SC _n -Hand-LT	AFI \gg CHA	0.805	59.4	6.02
Fe ₄ SC _n -Mech	AFI + dense phase	–	21.9	–
Fe ₄ SC _m -Hand	AFI + CHA	–	26.8	–
FeAPO-5-Hydro	AFI	0.478	44.8	0.42

^a Fe₁, Fe₂, Fe₃ and Fe₄ represent ferric nitrate, ferric chloride, ammonium ferric citrate and ferric citrate, respectively; SC_n and SC_m (type of seed crystal) are seed crystals of nanometer level and micrometer level, respectively

^bThe diffraction peak intensity ratio

^cDetermined by ICP-AES

Emission Spectrometry (ICP-AES) measurement. Diffuse reflectance UV–Vis spectra (DR UV–Vis) were measured with a spectrometer of Varian Gary 500, and BaSO₄ was used as an internal standard sample. CHN analysis was carried out on an Elemental Vario EL analyzer. Thermogravimetric (TG) and differential thermal analysis (DTA) (Netzsch, STA409) were performed in air at a heating rate of 10 °C/min.

Catalytic reaction

In a standard reaction, 2 g of phenol and 0.10 g of FeAPO-5 catalyst were added to 24 mL of deionized water in a three necks flask equipped with a magnetic stirrer and a reflux condenser. After heating the reaction mixture to 50 °C, 2.22 mL of hydrogen peroxide (H₂O₂, 30 wt% in water) was added through a syringe to the phenol solution containing catalyst (molar ratio of phenol/H₂O₂ = 1/1). The product distributions were determined by a LC2000 HPLC (Tianmei, Shanghai, China) equipped with a reversed phase C18 column using the methanol/water mixture (43/57, volume ratio) as the mobile phase at the flow rate of 1.0 mL min⁻¹ with UV detection at 277 nm.

Results and discussion

The effect of iron sources

For the synthesis of FeAPO-5 molecular sieves, the selection of iron sources is of paramount importance. Fig. 1 shows the XRD patterns of the samples synthesized with four different iron compounds as the iron sources. All samples present the fingerprint peaks associated with the AFI-type framework at $2\theta = 7.5^\circ, 14.9^\circ, 19.8^\circ, 21.1^\circ, 22.5^\circ$ and 26.0° . However, only the sample (Fe₄-Hand) using ferric citrate as the iron source reveals relatively pure AFI phase and higher crystallinity while other three samples contain minor impurities such as dense phase or CHA zeolite. This

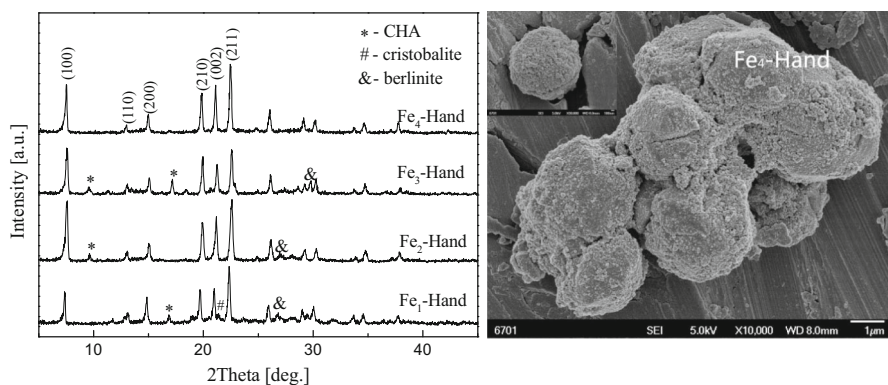


Fig. 1 XRD patterns and SEM images of FeAPO-5 samples synthesized under the conditions of different iron sources

may be due to the higher reactivity of the monomeric Fe source (ferric citrate) towards H_3PO_4 or pseudo-boehmite, compared with the polymeric Fe source (ferric nitrate, ferric chloride and ammonium ferric citrate). Apparently, the suitable iron source is ferric citrate for the solvent-free synthesis of FeAPO-5 . It should be noted that the use of solid state compound dipropylamine phosphate ($\text{DPA}\cdot\text{H}_3\text{PO}_4$), as indicated by Xiao [15], was very important for the solvent-free synthesis of aluminophosphate zeolites, but seemed to be not necessary in our case. Obviously, the synthesis procedure presented here is more convenient than the original one [15]. SEM images (Fig. 1) show that this sample $\text{Fe}_4\text{-Hand}$ is comprised of rough hamburger-like crystals. This peculiar morphology is quite distinct from that of the sample FeAPO-5-Hydro by conventional hydrothermal synthesis (Fig. 2), implying that the two samples were crystallized according to different growth mechanism.

The effect of low-temperature pretreatment

Crystallization temperature has a great influence on the zeolite nucleation and growth rate. In a case study of MFI zeolite synthesis, it was found that the aging of amorphous gel at low temperature can increase the number of nuclei [25]. In our work, the effect of low-temperature pretreatment on the synthesis of FeAPO-5 zeolite was investigated. In this synthesis, the precursor mixtures were first pretreated at a low temperature of 80°C before elevated temperature crystallization, which aim is to accelerate the generation process of nuclei and short the induction period of crystallization. The resulting product (Fig. 2, sample $\text{Fe}_4\text{-Hand-LT}$) is still pure AFI phase, but unexpectedly, with slightly lower crystallinity as compared to the sample $\text{Fe}_4\text{-Hand}$. This result could be attributed to the reason that the aging conditions employed here may be not suitable for the solvent-free synthesis of AFI

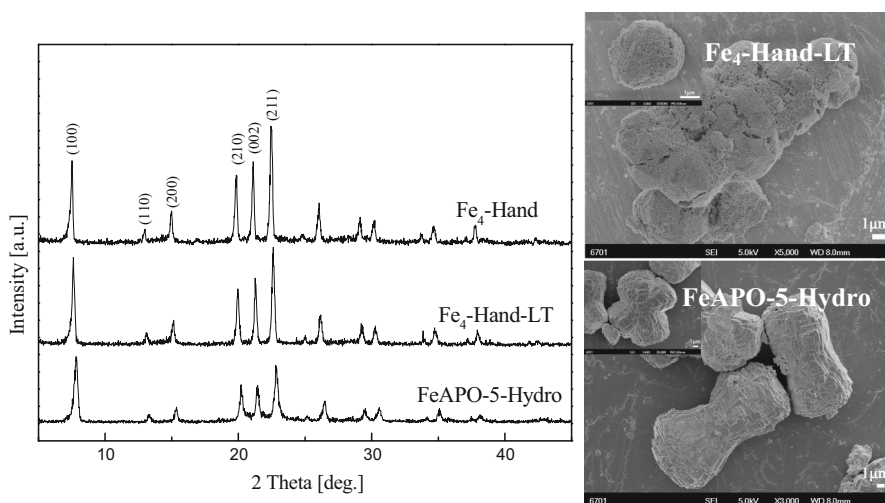


Fig. 2 XRD patterns and SEM images of FeAPO-5 samples synthesized under the conditions of low-temperature pretreatment, together with those of controlled samples

phase. In other words, under some cases gel aging has a great influence on the selectivity of zeolite crystals. Nevertheless, the crystallinity of Fe₄-Hand-LT is still higher than the sample FeAPO-5-Hydro. From the SEM images shown in Fig. 2, it is observed that the morphology of the sample Fe₄-Hand-LT is quite similar to that of the sample Fe₄-Hand, which shows that aging did not markedly influence morphology of the FeAPO-5 crystals, and also indicating that the two samples follow the same growth mechanism, i.e. a self-assembly mechanism involving the formation of a key intermediate consisting of 4-/6-MR chains according to Xiao's recent study [14].

The effect of mechanochemical treatment

In our previous research, it was found that the solvent-free synthesis of AFI- and AEL-type aluminophosphate molecular sieves from mechanochemically pretreated reactants displayed many advantages, such as the improved phase purity and reduced consumption of the structure-directing agents (SDA). Motivated by our previous study and the preparation of Silicalite-1 zeolites with high manganese contents [19], herein we modified the pretreatment procedure of FeAPO-5, aiming at obtaining a FeAPO-5 material with high iron content. First, the precursor mixtures with the composition of 1.0 Al₂O₃:0.762 P₂O₅:0.1 Fe₂O₃ were ball-milled to form a Fe–Al–P composite, then DPA and TEABr as the SDA were added to above precursor mixtures, followed by being ground in a mortar. The major phase of the resulting product is still AFI phase (Table 1 and Fig. S1, sample Fe₄-Mech), but with low crystallinity as compared with the sample Fe₄-Hand. What's more, considerable amounts of impurity phase such as cristobalite and CHA phase can be clearly observed in this sample. This result, especially the appearance of impurity phase, is however not anticipated, which may be explained by the fact that SDA molecules cannot be easily incorporated into the stable Fe–Al–P composite. It can also be speculated that the reason is that the precursor is partially deactivated after mechanochemical treatment. In view of the poor quality of the sample Fe₄-Mech, its iron content is thus not measured by ICP-AES.

The effect of H₂O₂

The introduction of hydroxyl free radical via physical or chemical methods has been shown to accelerate crystal crystallization in zeolite synthesis [21]. Thus, in the following syntheses, H₂O₂ was introduced to the synthesis mixture in order to improve the crystallinity of FeAPO-5 zeolite. As shown in Fig. 3 and Table 1, the major product is AFI phase accompanied by minor berlinite and CHA phase (sample Fe₄HP-Hand), and its crystallinity becomes lower in comparison with the sample Fe₄-Hand. In addition, the combining effects of H₂O₂ with mechanochemical or low-temperature pretreatment on the synthesis of FeAPO-5 zeolite were also investigated (samples Fe₄HP-Mech and Fe₄HP-Hand-LT), respectively. It can be seen that the sample Fe₄HP-Mech exhibits low crystallinity and contains large amounts of impurity phase, while the sample Fe₄HP-Hand-LT reveals relatively pure AFI phase with the highest crystallinity, only minor impurity phase at

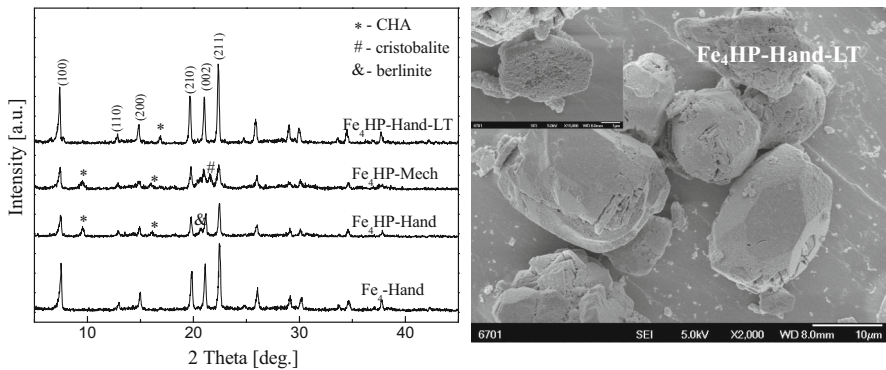


Fig. 3 XRD patterns and SEM images of Fe₄PO-5 samples synthesized in the presence of H₂O₂

$2\theta = 16.9^\circ$ is detected in this sample. According to work of Yu's group, hydroxyl free radical produced by Fenton reagent can significantly promote the crystallization of zeolites [21]. It is well known that the self-decomposition of H₂O₂ to water occurs at high temperature. Meanwhile H₂O₂ is decomposed into •OH in the process of low-temperature pretreatment, which thus leads to the high crystallinity of the sample Fe₄HP-Hand-LT. As can be seen from Figs. 1 and 3, the morphologies of Fe₄-Hand and Fe₄HP-Hand-LT are different from each other. The sample Fe₄HP-Hand-LT is comprised of smooth pebble-like crystals, wherein hexagonal crystal surface typical of the feature of AFI phase can be clearly observed, verifying its high crystallinity.

The effect of seed crystals

Seed crystals were introduced to the synthesis mixture in order to accelerate the crystallization process and control the phase purity of the products. As can be seen from Fig. 4 and Table 1, the major product is AFI phase accompanied by minor CHA phase when no pretreatment process is mediated but nanometer sized seed crystals are added to the reaction system (sample Fe₄SC_n-Hand). Likewise, pure AFI phase was not obtained when the synthesis gel was subjected to the mechanochemical or low-temperature pretreatment (sample Fe₄SC_n-Mech and Fe₄SC_n-Hand-LT). Among them, the sample Fe₄SC_n-Hand-LT reveals slightly higher crystallinity than the other two samples. It should be noted that the crystallinities of all samples synthesized in the presence of seed crystals are obviously lower than those in the absence of seed crystals (Fe₄SC_n-Hand vs. Fe₄-Hand, Fe₄SC_n-Mech vs. Fe₄-Mech, Fe₄SC_n-Hand-LT vs. Fe₄-Hand-LT). The SEM images shown in Fig. 4 indicate that the samples Fe₄SC_n-Hand and Fe₄SC_n-Hand-LT are composed of mixtures of rough sandwich-like crystals and irregular nanoparticles. As a comparison, micrometer sized seed crystals are added into the synthesis mixture to synthesize FeAPO-5 materials. As expected, the AFI phase in the obtained products (Fig. 4, sample Fe₄SC_m-Hand) exhibits much lower crystallinity in comparison with the sample Fe₄SC_n-Hand owing to the large size

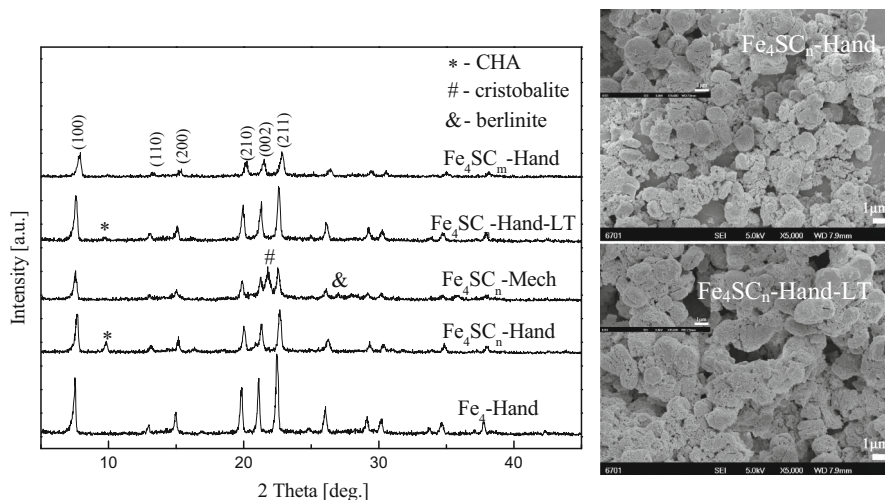


Fig. 4 XRD patterns and SEM images of FeAPO-5 samples synthesized in the presence of seed crystals

of the seed crystals. The above results suggest that the addition of seed crystals seems to have an unfavorable influence on the phase purity and crystallinity of the resulting products, which is in agreement with our previous study [18]. However, ongoing investigations in the author's laboratory demonstrated that the crystallinity of AEL- and CHA-type aluminophosphate molecular sieves could be improved by using ball-milled or chemically etched nano-sized seed crystals. Obviously, the decreased crystallinity observed in the seeded samples can be attributed to the reason that the added seed crystals were not activated by the precursor mixture during the synthesis.

Composition and structural analysis

Five representative AFI samples ($\text{Fe}_4\text{-Hand}$, $\text{Fe}_4\text{-Hand-LT}$, $\text{Fe}_4\text{HP-Hand-LT}$, $\text{Fe}_4\text{SC}_n\text{-Hand}$ and $\text{Fe}_4\text{SC}_n\text{-Hand-LT}$) and the controlled sample (FeAPO-5-Hydro) were analyzed by various techniques. Fig. 5 displays the nitrogen physisorption isotherms of abovementioned six samples, and their textural parameters are listed in Table 2. The type I adsorption isotherms of these materials imply that they are typical microporous materials. The appearances of hysteresis loops in the isotherms of the samples prepared by the solvent-free route demonstrate that they have minor additional mesopores or macropores. As a comparison, the sample FeAPO-5-Hydro is a typical microporous material, whose mesoporous volume is much lower than the other five samples. The pore size distributions (Fig. S2) of the samples $\text{Fe}_4\text{-Hand}$ and $\text{Fe}_4\text{-Hand-LT}$ determined from the adsorption branch of the isotherms, show two maxima, a relatively broad one usually centered at about 8 nm, representing the mesopores, and the other one at about 75 nm, which is attributed to the macropores. ICP-AES measurements demonstrate that the samples synthesized by the solvent-free method, without exception, exhibit much higher iron content than the

Fig. 5 N₂ adsorption/desorption isotherms of six representative FeAPO-5 samples. **a** FeAPO-5-Hydro; **b** Fe₄-Hand; **c** Fe₄-Hand-LT; **d** Fe₄HP-Hand-LT; **e** Fe₄SC_n-Hand; **f** Fe₄SC_n-Hand-LT

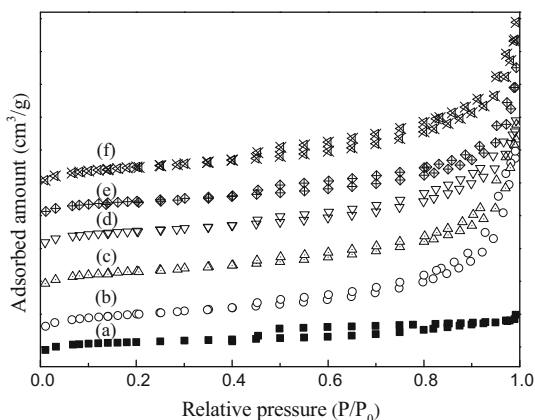


Table 2 Textural parameters of six representative FeAPO-5 samples

Sample	BET surface area (m ² /g)	Micropore surface area (m ² /g)	External surface area (m ² /g)	Micropore volume (cm ³ /g) ^a	Mesopore volume (cm ³ /g) ^b
Fe ₄ -Hand	241	177	64	0.082	0.225
Fe ₄ -Hand-LT	259	197	62	0.092	0.205
Fe ₄ HP-Hand-LT	251	194	57	0.091	0.160
Fe ₄ SC _n -Hand	279	224	55	0.105	0.185
Fe ₄ SC _n -Hand-LT	271	203	68	0.095	0.205
FeAPO-5-Hydro	268	240	28	0.112	0.045

^a t-plot micropore volume

^bBJH adsorption cumulative volume of pores between 1.7 nm and 300 nm

hydrothermally synthesized one (Table 1). Especially, the sample Fe₄-Hand displays the highest iron content (6.08 wt%) among these samples, which means that the solvent-free route is particularly suitable for synthesizing hierarchical porous zeolites with high metal content. From the above results, it can be seen that the samples Fe₄-Hand, Fe₄-Hand-LT and Fe₄HP-Hand-LT exhibit not only hierarchical porous structure, but also much higher iron content and crystallinity than the hydrothermal synthesized sample FeAPO-5-Hydro, which implies that these materials perhaps have a high potential in some industrially relevant applications.

TG–DTA measurements and CHN elemental analysis were used to determine the type and amount of organic amines occluded in the channels of FeAPO-5 samples. As shown in Fig. 6, the main weight loss accompanied by exothermic effect occurred in the temperature range of 330–550 °C, which can be ascribed to the combustion decomposition of SDA. For the samples Fe₄-Hand and Fe₄HP-Hand-LT, their weight losses are 7.55 wt% and 8.22 wt% in this step, respectively. CHN analysis indicates that the contents of C, H and N are 4.86 wt%, 1.80 wt% and 0.83

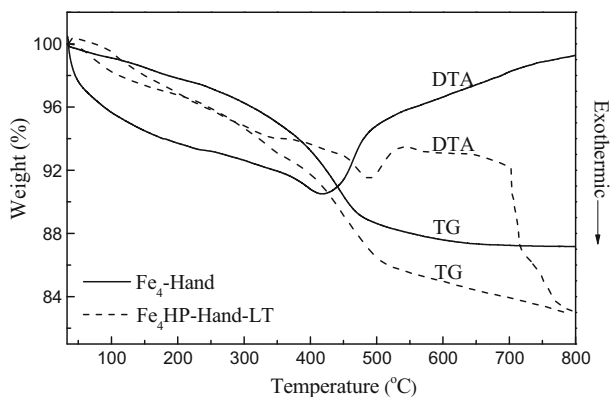


Fig. 6 TG–DTA curves of the as-synthesized FeAPO-5 samples

wt% in the sample Fe₄-Hand, while for the sample Fe₄HP-Hand-LT, the data are 5.27 wt%, 1.86 wt% and 1.00 wt%. Obviously, the CHN amounts are in good agreement with the weight loss in TG curves. Based on CHN analysis, the molar ratio of C/N of organic molecules occluded in the channels of Fe₄-Hand and Fe₄HP-Hand-LT can be calculated, which are 6.8 and 6.1, respectively. It is known that the molar ratio of C/N in DPA and TEABr molecules are 6 and 8, respectively. Thus, it can be conjectured from this result that DPA and TEABr molecules may co-direct the synthesis of Fe₄-Hand as also suggested by Xiao [15], while for Fe₄HP-Hand-LT, only DPA molecules play the role of SDA.

Coordination environment and distribution of iron species in FeAPO-5

Diffuse reflectance UV–Vis spectroscopy was commonly used to analyze the coordination environment and distribution of iron species in FeAPO-5 molecular sieves. Several characteristic UV–Vis absorption bands assigned to the specific ferric ion species were extracted from the UV–Vis spectra upon deconvolution (Figs. 7, S3), and their individual proportion thus can be estimated (Table 3). The specific ferric ion species mainly consist of isolated Fe³⁺ ions in tetrahedral coordination (two bands at 210 and 270 nm), small oligonuclear Fe_xO_y clusters in the zeolite channel and surface (the band at about 380 nm) and Fe₂O₃ nanoparticles at the external surface of zeolite crystals (the bands above 400 nm, centered at 470 and 520 nm) [26–29]. For FeAPO-5 samples obtained by solvent-free synthesis method, all above three types of iron species can be detected, whereas only isolated Fe³⁺ species were detected in the sample FeAPO-5-Hydro.

Catalytic testing of FeAPO-5 in phenol hydroxylation

Iron-containing molecular sieves are well known as active and selective catalysts for many oxidation reactions, among which the phenol hydroxylation is supposed to be very sensitive to framework iron species. In the past several decades, the

Fig. 7 UV–Vis diffuse reflectance spectra of six representative FeAPO-5 samples. **a** Fe₄-Hand; **b** Fe₄-Hand-LT; **c** Fe₄HP-Hand-LT; **d** Fe₄SC_n-Hand; **e** Fe₄SC_n-Hand-LT; **f** FeAPO-5-Hydro

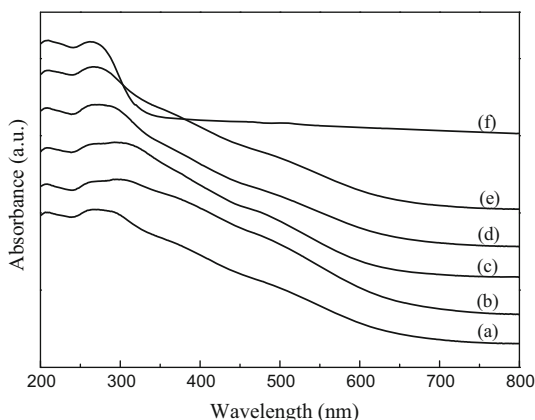


Table 3 Percentage of subband areas derived by deconvoluting UV–Vis spectra and corresponding Fe species loading

Sample	Isolated Fe ³⁺		Oligonuclear Fe _x O _y	Fe ₂ O ₃ nanoparticles		Isolated (wt%)	Oligonuclear (wt%)	Nanoparticles (wt%)
	A1 (%)	A2 (%)	A3 (%)	A4 (%)	A5 (%)			
Fe ₄ -Hand	13.36	35.03	18.68	24.26	8.67	3.266	1.136	2.002
Fe ₄ -Hand-LT	19.20	28.69	21.06	20.43	10.62	2.816	1.238	1.826
Fe ₄ HP-Hand-LT	11.55	42.96	21.31	15.40	8.78	2.780	1.087	1.233
Fe ₄ SC _n -Hand	18.72	29.29	23.84	16.33	11.82	2.593	1.287	1.520
Fe ₄ SC _n -Hand-LT	16.47	21.83	34.16	16.03	11.51	2.306	2.056	1.658
FeAPO-5-Hydro	53.95	46.05	~ 0	~ 0	~ 0	0.422	~ 0	~ 0

A1 and A2 represent the percentage of subband area at 210 and 270 nm, respectively

A3 represents the percentage of subband area at 380 nm

A4 and A5 represent the percentage of subband area at 470 and 520 nm, respectively

hydroxylation of phenol has been carried out over different iron-based zeolitic catalysts including Fe-MCM-41 [30], Fe-MFI [31], Fe/HBEA [32], Fe/Al-MCM-41 [33], nanocrystals Fe/KL [34], mesoporous and microporous Fe/NaY [35], and hierarchical structured FeAPO-5 [36]. From the above results, it was found that the presence of mesopores in the supports can significantly enhance mass transport, thus leading to short induction periods and high product selectivity.

In the current work, the hydroxylation of phenol with hydrogen peroxide was carried out to evaluate and compare the catalytic performances of representative FeAPO-5 catalysts with different iron content and textural parameters. This reaction has been known to proceed via the electrophilic substitution mechanism (Fig. S4), in which phenol reacted with hydroxyl radicals generated from Fenton's reaction over Fe oxides [30]. •OH attacks on the o- and p-position versus the OH group in the aromatic ring [30, 37, 38]. The main products of this reaction, i.e. catechol (CAT) and hydroquinone (HQ), have great importance in fine chemicals synthesis [32, 39].

Because the size of phenol molecule (0.7 nm) is slightly smaller than that of the micropores of FeAPO-5 molecular sieve (0.74 nm), phenol hydroxylation reactions largely take place in the channels of FeAPO-5 molecular sieve [40].

Five selected FeAPO-5 catalysts were tested in the phenol hydroxylation reaction, and the corresponding catalytic results are summarized in Table 4. These catalysts give phenol conversions of around 45% after 4 h reaction. However, various induction periods can be clearly observed for these catalysts. The samples Fe₄-Hand and Fe₄-Hand-LT exhibit relatively short induction time in comparison to the other three samples. The former two samples reached a stable phenol conversion in 3 h, while others needed 4 h. For this reaction, the induction period of 5–120 min was previously mentioned in the literature [41], which is strongly dependent on the framework iron species [30, 33]. For the samples Fe₄-Hand and Fe₄-Hand-LT, their relatively short induction period can be attributed to the higher framework iron content and the total iron content to some extent. Besides, the large mesoporous volumes of these samples usually facilitate the mass transfer of phenol and hydrogen peroxide to the active sites inside FeAPO-5 channels. As a result, hydroxyl radicals can be produced promptly and a short induction period was observed. For comparison purpose, the catalytic performance of the controlled sample (FeAPO-5-Hydro) with less than 1.00 wt% iron content was also investigated in the phenol hydroxylation reaction and a much longer induction period can be observed (Table S1). No any products were detected within 10 h reaction time. It can be seen from this result that the iron content also affects the catalytic activity and induction time.

It was reported that isolated tetrahedron coordinated iron species were the catalytic active centers for phenol hydroxylation with H₂O₂, while octahedron coordinated iron species were less active for this reaction [42–45]. As shown in Table 4, Fe₄-Hand-LT displays slightly lower phenol conversion and higher dihydroxybenzene selectivity than other catalysts. According to previous study, the low catalytic activity of Fe₄-Hand-LT catalyst can be explained by its high density of framework iron species [46, 47]. It should be noted that phenol conversion over Fe₄-Hand is comparable to the other three catalysts (Fe₄HP-Hand-LT, Fe₄SC_n-Hand, Fe₄SC_n-Hand-LT), although the former exhibits the highest density of framework iron species. For Fe₄-Hand catalyst, the active framework iron species inside its channels may be partly covered by the extra-framework iron species, as can be inferred from its lower microporous surface area, thus leading to decline of actual density of framework iron species.

According to the previous report, the diffraction peak intensity ratio of I₀₀₂/I₁₀₀ increased as the aspect ratio of the crystals decreased for AFI zeolite [48]. Lower aspect ratio means relatively short diffusion paths, which is favorable for the rapid diffusion of product molecules and preventing the secondary reactions of products in the channels. As shown in Table 1, the ratios of I₀₀₂/I₁₀₀ of the samples (Fe₄-Hand, Fe₄-Hand-LT and Fe₄HP-Hand-LT) are obviously higher than Fe₄SC_n-Hand. Thus, we can observe that dihydroxybenzene selectivity over the former three catalysts is relatively high (Table 4). For Fe₄SC_n-Hand-LT, although its I₀₀₂/I₁₀₀ ratio is also larger than that of Fe₄SC_n-Hand, the dihydroxybenzene selectivity over the two catalysts is similar. It was observed that the amount of nonselective active

Table 4 Effect of reaction time on phenol hydroxylation over five FeAPO-5 catalysts with different iron content

Catalyst	D.F.I. (10^{-4} g m $^{-2}$)	Time (h)	X_{ph} (%)	Y_{DHB} (%)	Product selectivity	
					(CAT + HQ) (%)	HQ/CAT
Fe $_4$ -Hand	1.84	0.5	1.1	0	0	–
		1	1.4	0	0	–
		2	3.8	0.2	4.8	0.2
		3	42.5	32.1	75.6	1.00
		4	43.5	32.6	75.0	1.01
		5	44.9	32.9	73.3	1.02
Fe $_4$ -Hand-LT	1.43	0.5	7.4	0	0	–
		1	2.2	0	0	–
		2	3.6	0	0	–
		3	40.3	32.2	79.9	0.96
		4	40.7	32.9	80.9	0.98
		5	42.4	33.6	79.2	1.04
Fe $_4$ HP-Hand-LT	1.32	0.5	0.1	0	0	–
		1	1.1	0	0	–
		2	2.4	0	0	–
		3	3.1	0	0	–
		4	44.7	33.8	75.7	1.06
		5	45.3	34.5	76.1	1.10
Fe $_4$ SC $_n$ -Hand	1.15	0.5	5.3	0	0	–
		1	3.7	0	0	–
		2	3.4	0	0	–
		3	3.8	0	0	–
		4	45.2	31.4	69.5	0.98
		5	45.7	33.1	72.4	0.99
Fe $_4$ SC $_n$ -Hand-LT	1.13	0.5	6.3	0	0	–
		1	4.9	0	0	–
		2	7.8	0	0	–
		3	9.1	0.5	5.6	0.24
		4	46.5	32.2	69.3	0.96
		5	47.5	32.7	68.8	1.01

D.F.I the density of framework iron species of corresponding catalyst, which is defined as the ratio of the amount of framework iron to micropore surface area

X_{ph} conversion of phenol

Y_{DHB} yield of dihydroxybenzene

species (i.e. oligonuclear Fe $_x$ O $_y$ and Fe $_2$ O $_3$ nanoparticles) in the sample Fe $_4$ SC $_n$ -Hand-LT was apparently higher than Fe $_4$ SC $_n$ -Hand (Table 3), which may account for its low dihydroxybenzene selectivity. Among all catalysts investigated here, Fe $_4$ -Hand-LT, which has a high content of framework iron species, shows the best

catalytic performance in phenol hydroxylation reaction, giving 40.0% of phenol conversion with dihydroxybenzene selectivity of 80% at 50 °C within 3 h reaction time.

Conclusions

In conclusion, hierarchical porous FeAPO-5 catalysts with high iron content and crystallinity were successfully synthesized by a modified solvent-free method. The synthesis experiments suggest that low-temperature pretreatment towards H₂O₂-containing precursor mixtures can significantly improve the crystallinity of FeAPO-5 molecular sieve. On the other hand, the addition of nonactivated seed crystals and/or introduction of mechanochemical pretreatment exhibits no any beneficial effect on the phase purity and crystallinity of the resulting products obtained by solvent-free method. The FeAPO-5 catalyst with a high content of framework iron species gives phenol conversions of up to 40% and dihydroxybenzene selectivity of 80% at mild reaction conditions. Although this catalytic result is not better than those iron-incorporated mesoporous molecular sieve catalysts reported in the literature, these FeAPO-5 catalysts may find potential applications in other reactions owing to their facile preparation and specific structure and properties.

Acknowledgements This work was supported by the National Natural Science Foundation of China (Grant No. 21306072 and 21666019) and the Natural Science Foundation of Gansu Province, China (Grant No. 17JR5RA124). We cordially thank the Reviewers and Editors for providing us with valuable comments and suggestions.

References

1. Wilson ST, Lok BMT, Messina CA, Cannan TR, Flanigen EM (1982) *J Am Chem Soc* 104:1146–1147
2. Flanigen EM, Lok BMT, Patton RL, Wilson ST (1986) *Pure Appl Chem* 58:1351–1358
3. Corma A (1997) *Chem Rev* 97:2373–2419
4. Davis ME (2014) *Chem Mater* 26:239–245
5. Davis ME, Saldarriaga C, Montes C, Garces JM, Crowder C (1988) *Nature* 331:698–699
6. Davis ME (2002) *Nature* 417:813–821
7. Miller SJ (1994) *Microporous Mater* 2:439–449
8. Feng P, Bu X, Stucky GD (1997) *Nature* 388:735–741
9. Bibby DM, Dale MP (1985) *Nature* 317:157–158
10. Morris RE, Weigel SJ (1997) *Chem Soc Rev* 28:309–317
11. Cooper ER, Andrews CD, Wheatley PS, Webb PB, Wormald P, Morris RE (2004) *Nature* 430:1012–1016
12. Wu Q (2012) Yinying, Ren L, Meng X, Xiao FS. *J Am Chem Soc* 134:15173–15176
13. Jin Y, Sun Q, Qi G, Yang C, Xu J, Chen F, Meng X, Deng F, Xiao FS (2013) *Angew Chem Int Ed* 52:9172–9175
14. Sheng N, Chu Y, Xin S, Wang Q, Yi X, Feng Z, Meng X, Liu X, Deng F, Xiao FS (2016) *J Am Chem Soc* 138:6171–6176
15. Jin Y, Chen X, Sun Q, Sheng N, Liu Y, Bian C, Chen F, Meng X, Xiao FS (2014) *Chem Eur J* 20:17616–17623
16. Zhao X, Zhao J, Wen J, An L, Li G, Wang X (2015) *Microporous Mesoporous Mater* 213:192–196
17. Zhao X, Zhao J, Gao X, Zhao Y (2015) *RSC Adv* 5:95690–95694
18. Zhao X, Gao X, Zhang X, Hao Z (2017) *Microporous Mesoporous Mater* 242:160–165

19. Iida T, Sato M, Numako C, Nakahira A, Kohara S, Okubo T, Wakihara T (2015) *J Mater Chem A* 3:6215–6222
20. Mintova S, Gilson JP, Valtchev V (2013) *Nanoscale* 5:6693–6703
21. Feng G, Cheng P, Yan W, Boronat M, Li X, Su JH, Wang J, Li Y, Corma A, Xu R (2016) *Science* 351:6
22. Iyoki K, Itabashi K, Okubo T (2014) *Microporous Mesoporous Mater* 189:22–30
23. Catana G, Pelgrims J, Schoonheydt RA (1995) *Zeolites* 15:475–480
24. Utchariyajit K, Wongkasemjit S (2010) *Microporous Mesoporous Mater* 135:116–123
25. Auerbach SM, Carrado KA, Dutta PK (2003) *Handbook of zeolite science and technology*. Marcel Dekker, New York
26. Samanta S, Giri S, Sastry PU, Mal NK, Manna A, Bhaumik A (2003) *Ind Eng Chem Res* 42:3012–3018
27. Li Y, Feng Z, Lian Y, Sun K, Zhang L, Jia G, Yang Q, Li C (2005) *Microporous Mesoporous Mater* 84:41–49
28. Li LD, Shen Q, Yu JJ, Hao ZP, Xu ZP, Lu GQM (2007) *Environ Sci Technol* 41:7901–7906
29. Kumar MS, Schwidder M, Grünert W, Brückner A (2004) *J Catal* 227:384–397
30. Choi JS, Yoon SS, Jang SH, Ahn WS (2006) *Catal Today* 111:280–287
31. Wang J, Xu J, Li B, Zhang G, Wu N, Mao L (2014) *Mater Lett* 124:54–56
32. Kosri C, Deekamwong K, Sophiphun O, Osakoo N, Chanlek N, Föttinger K, Wittayakun J (2017) *React Kinet Mech Catal* 121:751–761
33. Preethi MEL, Revathi S, Sivakumar T, Manikandan D, Divakar D, Rupa AV, Palanichami M (2008) *Catal Lett* 120:56–64
34. Adam F, Wong JT, Ng EP (2013) *Chem Eng J* 214:63–67
35. Mohamed MM, Eissa NA (2003) *Mater Res Bull* 38:1993–2007
36. Zhao X, Sun Z, Zhu Z, Li A, Li G, Wang X (2013) *Catal Lett* 143:657–665
37. Chellal K, Bachari K, Sadi F (2014) *J Cluster Sci* 25:523–539
38. Liu C, Shan Y, Yang X, Ye X, Yue W (1997) *J Catal* 168:35–41
39. Khodadadi Z, Mahmoudian R (2016) *React Kinet Mech Catal* 119:685–697
40. Kamegawa T, Ando T, Ishiguro Y, Yamashita H (2015) *Bull Chem Soc Jpn* 88:572–574
41. Jin M, Yang R, Zhao M, Li G, Hu C (2014) *Ind Eng Chem Res* 53:2932–2939
42. Li B, Wu K, Yuan T, Han C, Xu J, Pang X (2012) *Microporous Mesoporous Mater* 151:277–281
43. Xin H, Liu J, Fan F, Feng Z, Jia G, Yang Q, Li C (2008) *Microporous Mesoporous Mater* 113:231–239
44. Liu H, Lu G, Guo Y, Guo Y, Wang J (2008) *Microporous Mesoporous Mater* 108:56–64
45. Li B, Xu J, Liu J, Pan Z, Wu Z, Zhou Z, Pang X (2012) *Mater Lett* 78:147–149
46. Zhao X, Zhang X, Hao Z, Gao X, Liu Z (2018) *J Porous Mater* 25:1007–1016
47. Wu C, Kong Y, Gao F, Wu Y, Lu Y, Wang J, Dong L (2008) *Microporous Mesoporous Mater* 113:163–170
48. Jung SH, Chang JS, Hwang YK, Park SE (2004) *J Mater Chem* 14:280–285